



OPEN

Study on influence of cosine-shaped subgrade settlement at different positions on the deformation and interlayer contact behavior of unit slab ballastless track

Jing Tan^{1,2}, Xuehui Jiang^{1,2}, Ruping Luo²✉, Hongyan Li³, Shuai He² & Yu Hou⁴

The influence of cosine-shaped subgrade settlement (CSSS) at different positions on the structure of unit slab ballastless track (USBT) of high-speed railway (HSR) is studied in this paper. The pre-developed general mapping model of the track structure deformation and interlayer contact behavior evolution of HSR is used, the CSSS description function is incorporated, and the deformation equations for each layer of the USBT structure under CSSS are derived. The incremental approach method is used to solve the statically indeterminate equation with contact nonlinearity, and then the influence of CSSS at different positions on the track structure deformation and interlayer contact behavior evolution is analyzed. The results show that the transfer pattern of track deformation is related to the position of settlement, and the structure deformation is more sensitive to the settlement at the position of the slab joint. Under the CSSS, the vertical deformation of the track structure remains synchronized and is transmitted upward layer by layer. The type of track irregularity differs between the subgrade settlement area and the area outside of it. In the area of uneven subgrade settlement and its small area on both sides, the debonding position of the track slab-base slab and track system-subgrade system mainly appears at the position of the slab joint, which presents the distribution law of “smaller at the near end, larger at the far end”.

Keywords Mapping model, Cosine-shaped subgrade settlement, Unit slab ballastless track, Track deformation, Contact behavior

The operation of high-speed rail (HSR) requires very high standards for the smoothness of its infrastructure¹. The subgrade settlement deformation will be uploaded to the rail surface layer by layer, so that the track system will produce following deformation and the original contact state between the track layers will change. Under the cyclic impact of the train, the interaction between the track system and the subgrade continues to deteriorate, accelerating the destruction of the balance between the subgrade and the track, which reduces the functionality and durability of the track structure and seriously endangers the stability and safety of the train^{2,3}.

Currently, many scholars have conducted research on the mapping analytical model of ballastless track structure deformation caused by foundation structure damage. Nie et al.⁴⁻⁶ studied the mapping analytical solution between the vertical deformation of the bridge and the vertical track irregularity using the stationary potential energy theory. Chen et al.⁷⁻⁹ proposed a mapping analytical solution method for pier settlement and track irregularity of simply supported beam bridge, and analyzed the dynamic change of interlayer contact behavior of the track structure. In order to predict the long-term track deterioration of ballastless track caused by the evolution of subgrade differential settlement of HSR, Guo et al¹⁰⁻¹² developed a calculation method to establish the mapping relationship between track irregularity and subgrade settlement, and compared and

¹Dept. of International Engineering, Jiangxi College of Foreign Studies, Nanchang 330099, China. ²School of Civil Engineering and Architecture, East China Jiaotong University, Nanchang 330013, China. ³Department of Electronics and Information Engineering, Nanchang Normal College of Applied Technology, Jiujiang 332000, China. ⁴Central South University, Changsha 410012, China. ✉email: 862122469@qq.com

analyzed the deformation characteristics and variation laws of two kinds of rail surface caused by different settlement types. Mićić M et al.¹³ established the relationship between track stiffness and the appearance and development of squat defects on running rails. The results indicated a correlation between the incidence of squats and the changes in track support stiffness. Zhang et al.¹⁴ established a mapping model to investigate the standard value of differential subgrade settlement and found that the longitudinal position of the settlement waveform is related to the interlayer connection of track structure. Zhong et al.¹⁵ proposed a spatial relation mapping model (SMRM) and analyzed the spatial geometry of the track under subgrade settlement.

In addition, some scholars have investigated the failure modes of the track and the interaction mechanisms under subgrade settlement through experiments or finite element modeling. In order to evaluate the impact of the lateral subgrade differential settlement, Cui et al.^{16,17} Cui developed a finite element model incorporating concrete material damage behavior and interlayer bonding forces, focusing on the analysis of rail deformation and concrete damage. Xu et al.¹⁸ established a 3D nonlinear static FEM, validated it using experimental data, and analyzed the forces exerted by the ballastless track slab on the subgrade under gravity, train, settlement, and temperature gradient. Sajjad M B. et al.¹⁹ found that the change of track stiffness will lead to accelerated aging of track materials and geometric shapes, resulting in reduced efficiency and shortened track life. Wang et al.²⁰ proposed an iterative approach to assess and forecast the track cumulative settlement, which involves finite element simulation and iterative calculation. Shan et al.²¹ introduced an iterative approach for investigating the deformation patterns of rails caused by foundation settlement in the road-bridge transition zone. Additionally, a cumulative plastic strain model for the soil was established to analyze the degradation process of uneven settlement in the transition zone. Heydari H et al.^{22–24} explored the dynamic performance of combined transition systems in slab-ballasted railway tracks through numerical modeling and field studies on the Tehran-Karaj railway line. Using 3D finite element vehicle-track-substructure interaction models validated against field measurements, they found that combined systems (auxiliary rails + approach slab) achieve smoother stiffness transitions through gradual steps, with optimal performance occurring at 4-step stiffness changing patterns and 20–25 m transition zone lengths, resulting in wheel-rail contact force reductions of up to 21% compared to cases without transition zones. Xiao²⁵ established a 3D finite element model for the CRTS III slab ballastless track system to investigate the deformation, stress, and interlayer contact state variations of the track under foundation settlement.

In summary, in the existing research system, the application of the mapping analytical method mainly focuses on the field of bridge structure, and its research focuses on the influence mechanism of bridge stiffness change on the force characteristics and deformation behavior of track structure. In contrast, for the deformation of the track system induced by subgrade settlement, the current research methods mainly present two paradigms: one is the empirical analysis based on the field measured data, which is reliable but has the economic problems of high cost and long cycle; the second is to use the predictive research of finite element numerical simulation. The calculation is more accurate but there are computational efficiency problems such as unadjustable parameters and long modeling time. In addition, there are still obvious deficiencies in the field of interlayer interaction of track structures, especially in the systematic research on key scientific issues such as interlayer contact mechanical behavior and dynamic evolution of contact state. For the unit slab ballastless track-subgrade system, there are few studies on the influence of subgrade settlement at different positions on the structural deformation of each layer of the track, the contact characteristics between the track slab-base slab and the track system-subgrade system. In view of this, combined with the structural characteristics of the unit ballastless track on the soil subgrade of domestic high-speed railway, based on the general mapping model of track structure deformation and interlayer contact characteristics evolution induced by the foundation deformation of high-speed railway developed in the early stage, an analytical model of unit slab ballastless track-subgrade was established, aiming to study the differential influence of different settlement positions on the deformation characteristics of each layer of the track structure, and further reveal the relationship between the interlayer contact force and contact characteristics of the unit slab ballastless track-subgrade system under each settlement position and the evolution law of interlayer contact characteristics.

Mapping model of structure deformation of each layer of the track and evolution of interlayer contact behavior under the action of CSSS

At present, the common uneven subgrade settlement is commonly categorized into “sudden-change type” and “slow type”. The mutant type can be described by angular and staggered curves, and the slow type is simulated by cosine curve. In this paper, the CSSS mode of is selected for research and analysis, as shown in Fig. 1.

As shown in Fig. 1, under the action of uneven subgrade settlement (USS), the USBT system produces following vertical deformation due to the self-weight of the structure, which causes the track irregularity. At the same time, due to the high stiffness and independence of the unit track structure, deformation of each structural layer in the track-subgrade system is not coordinated, leading to debonding between the structural layers in the USS area. When the high-speed train passes through these areas, the vertical acceleration, the wheel load reduction rate, the derailment coefficient and the vertical wheel-rail force of the vehicle body increase, thereby reducing the driving safety and comfort.

Function expressions can be used to simulate different deformation forms of subgrade. The expression of USS is as follows:

$$y_{bi} = - \frac{S}{2} \left(1 - \cos \frac{2\pi(l_{bi} - l_{b0})}{L} \right) \quad (1)$$

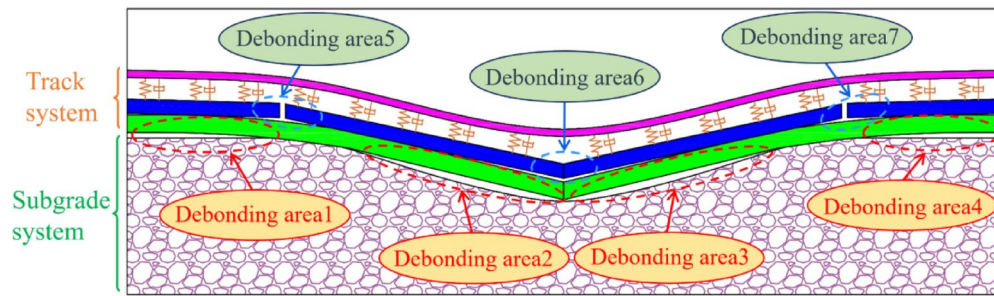


Fig. 1. Schematic diagram of CSSS description curve and its induced debonding of unit ballastless track-subgrade.

where y_{bi} represents the subgrade displacement at the position of i^{th} contact spring; S and L represent the amplitude and wavelength of the USS, with the value of L being 20 m in this paper.; l_{b0} represents the initial position of deformation; l_{bi} represents the position of i^{th} contact spring on the subgrade.

Through the above analysis, based on the pre-developed general mapping model of the track structure deformation and interlayer contact behavior evolution induced by foundation deformation of HSR^{26,27}, the expression of USS in Eq. (1) is implanted into the general mapping model, and the mapping model of the deformation of each layer of the track structure and the evolution of interlayer contact behavior under the action of USS is established as follows:

$$\begin{cases} \mathbf{V}_r = \mathbf{AF} + \mathbf{BQ}_r \\ \mathbf{V}_s = \mathbf{C}_1 \mathbf{F} + \mathbf{C}_2 \mathbf{P} + \mathbf{DQ}_s + \mathbf{R} \\ \mathbf{V}_p = \mathbf{H}_1 \mathbf{P} + \mathbf{H}_2 \mathbf{N} + \mathbf{IQ}_p + \mathbf{U} \end{cases} \quad (2)$$

Where \mathbf{V}_r , \mathbf{V}_s , \mathbf{V}_p represent the deformation matrix of rail, track slab and base plate respectively; \mathbf{A} , \mathbf{B} , \mathbf{C}_1 , \mathbf{C}_2 , \mathbf{D} , \mathbf{H}_1 , \mathbf{H}_2 , \mathbf{I} represent the influence matrix of the deformation; \mathbf{Q}_r , \mathbf{Q}_s , \mathbf{Q}_p represent the weight matrix; and \mathbf{F} , \mathbf{P} , \mathbf{N} represent the spring force matrix of each layer of the track respectively; \mathbf{R} is the influence matrix of base slab deformation on the vertical deformation of track slab; \mathbf{U} is the influence matrix of foundation damage deformation on the vertical deformation of the base slab. The expression of each influence matrix is similar to that of the rail, so they are not listed. the expressions are as follows :

$$\begin{cases} \mathbf{F} = \mathbf{k}_c (\mathbf{V}_s - \mathbf{V}_r) \\ \mathbf{P} = \mathbf{k}_{ca} (\mathbf{V}_p - \mathbf{V}_s) \\ \mathbf{N} = \mathbf{k}_p (\mathbf{V}_b - \mathbf{V}_p) \end{cases} \quad (3)$$

where \mathbf{k}_c , \mathbf{k}_{ca} , \mathbf{k}_p represent the stiffness matrix of fastener spring, mortar spring and contact spring respectively; \mathbf{V}_b represents the deformation matrix of the USS, which is constructed by Eq. (1).

To solve Eq. (2) ~ (3) simultaneously, the structure deformation of each layer of the track can be expressed as:

$$\begin{bmatrix} \mathbf{V}_r \\ \mathbf{V}_s \\ \mathbf{V}_p \end{bmatrix} = \begin{bmatrix} \mathbf{E} + \mathbf{k}_c \mathbf{A} & -\mathbf{k}_c \mathbf{A} & 0 \\ \mathbf{k}_c \mathbf{C}_1 & \mathbf{E} - \mathbf{k}_c \mathbf{C}_1 + \mathbf{k}_{ca} \mathbf{C}_2 & -\mathbf{k}_{ca} \mathbf{C}_2 \\ 0 & \mathbf{k}_{ca} \mathbf{H}_1 & \mathbf{E} - \mathbf{k}_{ca} \mathbf{H}_1 + \mathbf{k}_p \mathbf{H}_2 \end{bmatrix}^{-1} \begin{bmatrix} \mathbf{BQ}_r \\ \mathbf{DQ}_s + \mathbf{R} \\ \mathbf{k}_p \mathbf{H}_2 \mathbf{V}_b + \mathbf{IQ}_p + \mathbf{U} \end{bmatrix} \quad (4)$$

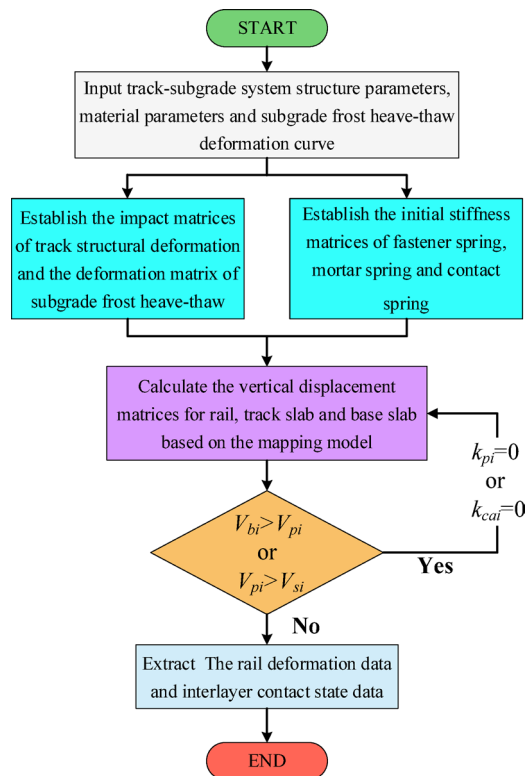
where, \mathbf{E} represents the unit matrix.

In addition, due to the contact nonlinearity between the track structural layers, it cannot be solved directly. Therefore, the Heaviside function is introduced to form a tension-free Winkler beam, which is used to describe the nonlinear contact relationship between the track system and the subgrade system.

$$T = \begin{cases} 1, & y_{up} - y_{do} > 0 \\ 0, & y_{up} - y_{do} \leq 0 \end{cases} \quad (5)$$

Where y_{up} represent the deformation of the upper structure; y_{do} represent the deformation of the lower structure. The incremental approach method is used to solve the statically indeterminate Eq. (5) with contact nonlinearity^{26,27}, and the calculation flow chart is shown in Fig. 2, which mainly introduces the calculation process of track regularity and interlayer contact characteristics:

1. Input structural parameters (including geometric parameters of each layer structure, fastener spacing, number of fasteners, etc.), material parameters (including bending stiffness of each layer structure, elastic modulus, vertical stiffness of interlayer spring, etc.) and subgrade settlement deformation curve data;
2. Establish the influence matrix of the structural deformation of each layer of the track, the initial stiffness matrix of the interlayer spring and the subgrade settlement deformation matrix \mathbf{V}_b ;

**Fig. 2.** Calculation flowchart.

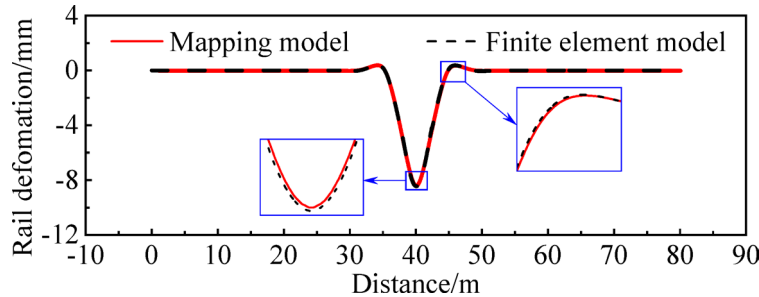
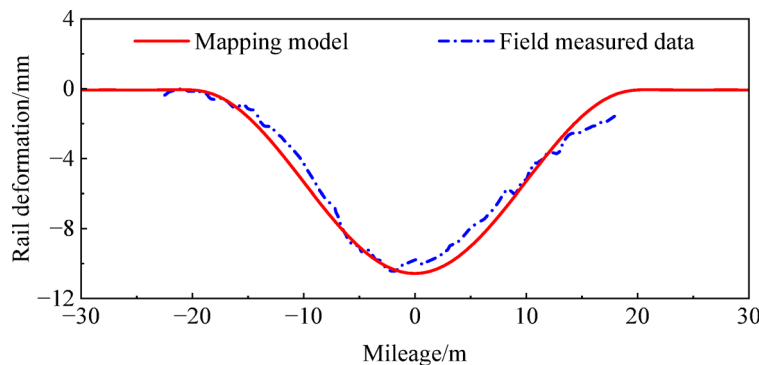
Structure	Thickness (m)	Elastic modulus (MPa)	Poisson ratio	Density (kg·m ⁻³)	Internal friction angle (°)	Cohesive force (kPa)
Surface layer of subgrade bed	0.4	150	0.3	2100	30	10
Base layer of subgrade bed	2.3	120	0.3	2000	20	15
Embankment under subgrade bed	4	80	0.3	1900	15	20

Table 1. Subgrade system model component parameters.

3. Based on the deformation mapping model of the track-subgrade system, develop a calculation program by MATLAB numerical simulation platform (www.mathworks.com) and calculate the vertical displacement matrix of rail, track slab and base slab;
4. Judge the interlayer contact state and update the interlayer spring stiffness matrix by comparing the structural displacement. Specifically, when the subgrade settlement displacement is greater than the displacement of the base slab, there is a void between the two layers, and the contact spring in the void area fails with a stiffness of 0. When the displacement of the base slab is greater than the displacement of the track slab, the force transmission characteristics of the mortar layer fail, and the stiffness of the mortar spring at the failure position is 0. Through multiple iterations, until the interlayer spring stiffness matrix no longer changes;
5. Output track irregularity data and interlayer contact state data and the solution is completed.

Unit slab ballastless track adopts the following structural forms and material configurations: the rail is 60 kg/m rail used in China's high-speed railway, with J-7B fastener. The adjustment layer employs CA mortar layer, the track slab material adopts C60 concrete, the convex retaining platform and base slab adopt C40 concrete, and other input parameters are shown in Tables 1 and 2. The FEM of the track-subgrade system is established by using the finite element software ANSYS, in which the rail, track slab, base slab and subgrade are simulated by three-dimensional beam element BEAM188, the fastener, mortar layer and contact layer are simulated by COMBIN39 spring element, and the connection between the main node and the slave node is simulated by MPC184 rigid beam element. In order to ensure the calculation efficiency and accuracy, the mesh size is 1/20 of the fastener spacing. Based on the Eq. (1), the cosine settlement deformation is applied to the subgrade, and the longitudinal length of the model is taken as 80 m to fully reflect the influence of the subgrade settlement range and eliminate the boundary effect. The results of the mapping model are compared with those of the finite element analysis. As

Structure	Thickness/m	Elastic modulus/MPa	Poisson ratio	Density/(kg·m ⁻³)
Rail	U71MnG	2.10×10^5	3.217×10^7	—
Fastener	WJ-7B	—	—	$3.0 \times 10^7 \text{ N/m}$
Track slab	C60 concrete	3.65×10^4	1.372×10^9	—
Mortar layer	CA mortar	2.00×10^2	—	$9.0 \times 10^8 \text{ N/m}$
Base slab	C40 concrete	3.40×10^4	1.867×10^9	—

Table 2. Track system model components parameters.**Fig. 3.** Mapping model and finite element model validation.**Fig. 4.** Mapping Model and Measured Data Validation.

shown in Fig. 3, the two calculation results are in good agreement (error between the two $< 1\%$). It shows that the general mapping model is still applicable after the description function of the USS is implanted.

Taking the measured data of the vertical rail deformation in the differential subgrade settlement section on a high-speed railway line measured by the rail inspection vehicle in Reference²⁸, and the corresponding vertical rail deformation calculated by the mapping model is compared with it, as shown in Fig. 4. It can be seen that the measured data curve is in good agreement with the trend of the data curve calculated by the mapping model. To a certain extent, it shows the reliability of the model in this paper.

Influence of USS at different positions on the deformation of each layer of track structure

The USBT on the subgrade is primarily categorized into two types: 10 m long base slab (laying 2 track slabs, referred to as A-type track structure) and 20 m long base plate (laying 4 track slabs, referred to as B-type track structure). In this paper, the B-type track structure is chosen as the focus of the study, and the track-subgrade coupling system with the length of 5 base slabs is taken as the calculation case. For the USBT with the high independence of track slab and base slab, the deformation of the track structure and the interlayer interaction may vary depending on the different positions of the USS. Therefore, by considering the positions of 1[#] (the base slab joint), 2[#] (the mid-span of the track slab between the C1 and C2 track slab joints), and 3[#] (the C3 track slab joint) as the positions of USS, the study investigates the impact of USS at different positions on the deformation of each layer within the track structure. The USS at different positions and the numbering of track slab joints are shown in Fig. 5.

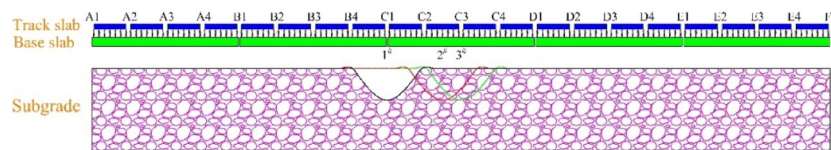


Fig. 5. Schematic diagram of USS and numbering of track slab joints at different positions.

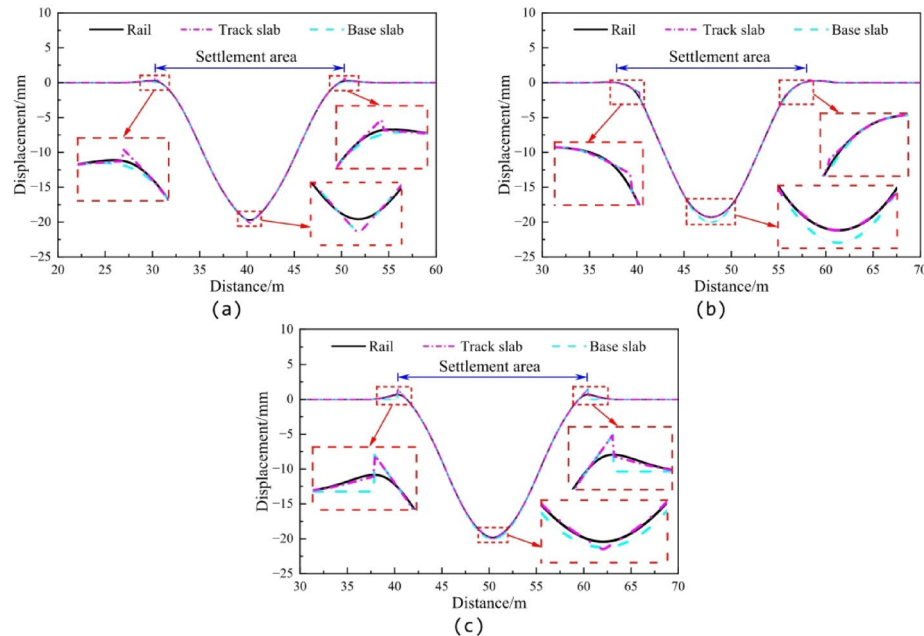


Fig. 6. Relationship between USS at different positions and vertical displacement of each layer of track structure. (a) Vertical displacement of the structure at 1# position, (b) Vertical displacement of the structure at 2# position, (c) Vertical displacement of the structure at 3# position.

Transfer law of USS-track deformation

The deformation transfer law of USBT under USS is analyzed using the established mapping model. The relationship between the USS at different positions and vertical displacement of each layer of the track structure is shown in Fig. 6.

As shown in Fig. 6, the transfer law of USS-track deformation is related to the position of settlement. When the uneven settlement deformation occurs at 1# position. At the peak settlement position, the linear deformation of the track slab and the base slab is concentrated in a small area on both sides of the joint between the slabs. In contrast, the rail deformation is relatively mild due to its higher structural integrity. In addition, the track slab has upwarping deformation at the position of the slab joint on both sides of the settlement area, which makes the deformation difference between the track slab and the base slab, resulting in the interlayer debonding. When the uneven settlement deformation occurs at 2# position, the deformation of rail, track slab and base slab remains gradual since the settlement amplitude does not coincide with the slab joint. However, in the left side of the settlement area, the deformation of the track slab and the base slab continues to be influenced by the slab joint. When the uneven settlement deformation occurs at 3# position, at the settlement amplitude position, the deformation difference between the track slab and the base slab is significantly smaller than that at 2# position. However, on both sides of the settlement area, the track slab and base slab exhibit a significant “sudden-change type” vertical deformation at the slab joint, indicating that the deformation of USS predominantly influences the structural deformation within the settlement area. On the whole, the structure deformation at the position of the slab joint is easily affected by the slab joint, and it is more likely to cause the deformation at the joint position to be inconsistent, resulting in the interlayer debonding. Therefore, when studying the influence of foundation damage on USBT, the influence of slab joint should be paid attention to.

Influence of the action position on the structure deformation

After the subgrade deformation, the vertical displacement of each layer of the track structure maintains good synchronization under the action of interlayer connection. The subgrade deformation is transferred to the rail layer by layer, and the track irregularity is formed. When the wavelength of USS is 20 m and the settlement

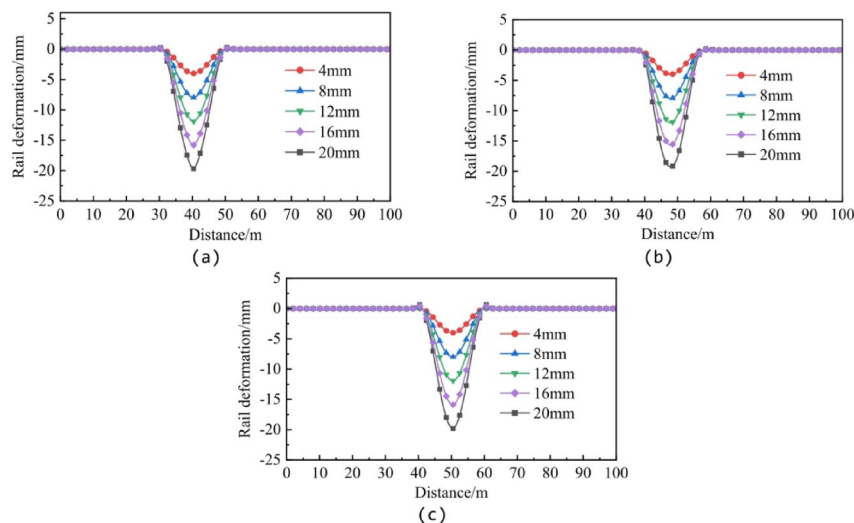


Fig. 7. Waveform curves of track irregularity under subgrade settlement at different positions. (a) Track irregularity at 1# position, (b) Track irregularity at 2# position, (c) Track irregularity at 3# position.

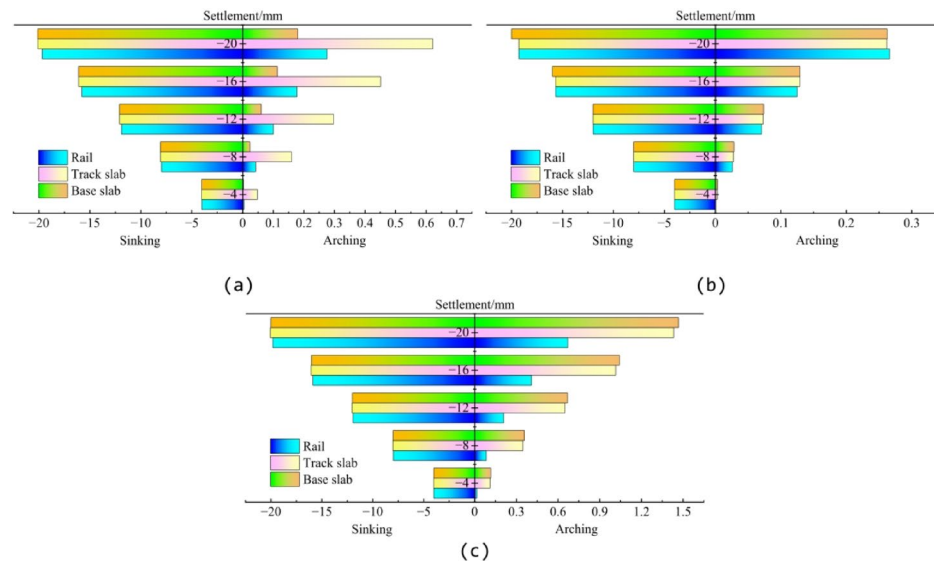


Fig. 8. Maximum deformation of each layer of the track structure under the subgrade settlement at different positions. (a) 1# position, (b) 2# position, (c) 3# position.

amplitude increases from 4 mm to 20 mm, the waveform curves of track irregularity at different positions are shown in Fig. 7.

As shown in Fig. 7, with the increase of subgrade settlement amplitude, the amplitude of track irregularity at different positions increases linearly. The impact of the position of USS on track deformation is also evident in track irregularity. In general, the track irregularity at different locations is shown as: in the area of USS, the type of track irregularity is the same as the USS, which is manifested as cosine type. The rail is uplifted at the edge of the settlement area outside the settlement area, and the arching deformation occurs, so that the wavelength of the rail deformation diffuses to both sides, and the diffusion speed exhibits a gradually decreasing nonlinear trend as the subgrade settlement amplitude increases.

Figure 7 shows that the USS will not only cause the sinking deformation of the rail in the settlement area, but also cause the rails on both sides of the settlement area to arch. Therefore, under the subgrade settlement, the maximum sinking and arching deformation of each layer of the track structure at different positions are extracted, and the direct impact of settlement position on each layer of the track structure is analyzed. The maximum deformation of each layer of the track structure under the subgrade settlement at different positions is shown in Fig. 8.

Figure 8 shows that as the settlement amplitude increases, the sinking and arching deformation of each layer of the track structure at 1#, 2# and 3# positions increase linearly and nonlinearly respectively. Under the

subgrade settlement at different positions, the rail deformation under the same settlement amplitude is relatively close, but the deformation of the track slab is very different from the deformation of the base slab. When the subgrade settlement occurs at 1[#] position, the subgrade settlement deformation amplitude is positioned at the joint between the track slab and the base slab. Consequently, the track slab and base slab deform in a coordinated manner due to the interlayer bonding force. But the track slab experiences significantly more pronounced arching deformation than the base slab. This is because within the small areas on either side of the subgrade settlement area, the base slab is longitudinally integral, and the deformation is mainly bending deformation. However, the track slab has slab joints in this range, and the deformation is not constrained by adjacent structures, so the arching deformation is very large. The sinking and arching deformation principle of the track structure under other subgrade action positions is similar to that at 1[#] position. In general, the position of subgrade settlement deformation has a significantly lesser impact on rail deformation compared to its effect on the track slab and base slab. Additionally, the deformation of both the track slab and base slab is influenced not only by the settlement position but also closely related to the slab joints. At the settlement amplitude and the positions on both sides of the settlement area, the deformation of the track slab and the base slab with the slab joint surpasses that of the entire longitudinal structure. Slab joints are a crucial factor contributing to the uncoordinated deformation of each layer of the track structure.

Influence of USS at different positions on the interlayer contact behavior of structure

When the USS occurs, the relative displacement difference will be generated between the structural layers, which will change the contact behavior between the upper and lower adjacent structures, thus causing a sudden change in interlayer force. Taking the USS of 20 m/20 mm (wavelength/settlement) at 1[#] position as an example, the change law of contact state between track slab-base slab and track system-subgrade system is analyzed. Figure 9 shows the correlation between the interlayer displacement difference and the interlayer force of the structure at 1[#] position. Among them, the interlayer force is positive.

From Fig. 9, it can be seen that the change of contact behavior between upper and lower adjacent structures only occurs in the area of USS and the small area on its both sides. The change types of contact behavior can be divided into separation debonding and extrusion contact. Among them, the debonding area primarily forms on either side of the slab joints, where the contact force drops to 0. The contact area mainly exists on both sides of the debonding area, and the deformation state shows that the downward deformation of the track exceeds the subgrade settlement value, so that the stress state of the track in this area mutates, resulting in a large upward support force. On the whole, when the uneven settlement occurs at 1[#] position, the debonding area between the track slab-base slab, the track system-subgrade system and the force curve of the track shows left-right symmetrical characteristics. In the contact area near the settlement center, there is a substantial displacement difference between the upper and lower adjacent structures, and the corresponding contact force is also large. In the contact area far away from the settlement center, the interlayer displacement difference between the upper and lower adjacent structures is small, and the corresponding contact force is also small.

Influence of USS on the contact behavior between the track slab and the base slab

Through the above analysis, it can be seen that the track slab and the base slab are prone to deformation inconsistency at the position of the slab joint, resulting in the interlayer debonding between the structural layers. To determine how the USS position affects interlayer debonding, a subgrade settlement wavelength of 20 m was utilized, and the settlement amplitude was varied from 4 mm to 20 mm. The influence of the position of USS on the contact behavior between the track-subgrade is studied. In view of the left-right symmetrical characteristics of the interlayer debonding area when the settlement occurs at 1[#] and 3[#] positions, only the left area of the settlement amplitude is analyzed. The longitudinal distribution of the debonding between the track slab-base slab under the subgrade settlement at different positions is shown in Fig. 10.

Figure 10 shows that when the subgrade settlement is at 1[#] position, an increase in settlement amplitude leads to a rise in both the height and length of interlayer debonding, and the debonding area gradually diffuses to both sides of the slab joint. However, in this process, the diffusion rate of the debonding area gradually decreases as the settlement amplitude increases. In addition, the height of the deboning near the position of the settlement

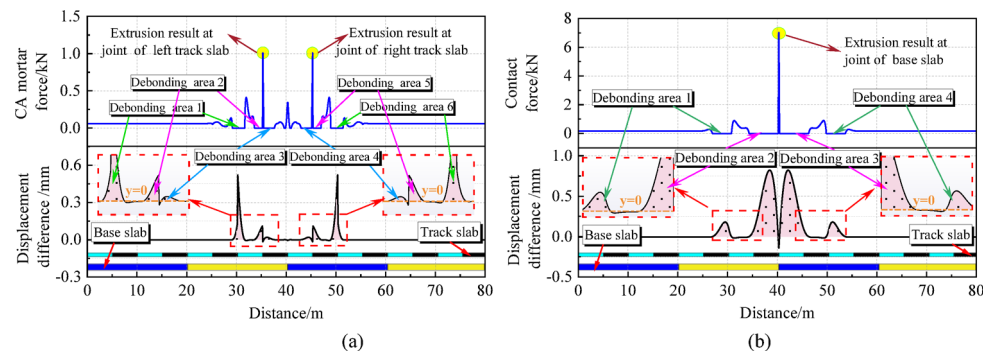


Fig. 9. Correlation between the Interlayer displacement difference and the interlayer force at 1[#] position. **(a)** Track slab-base slab, **(b)** Track system-subgrade system.

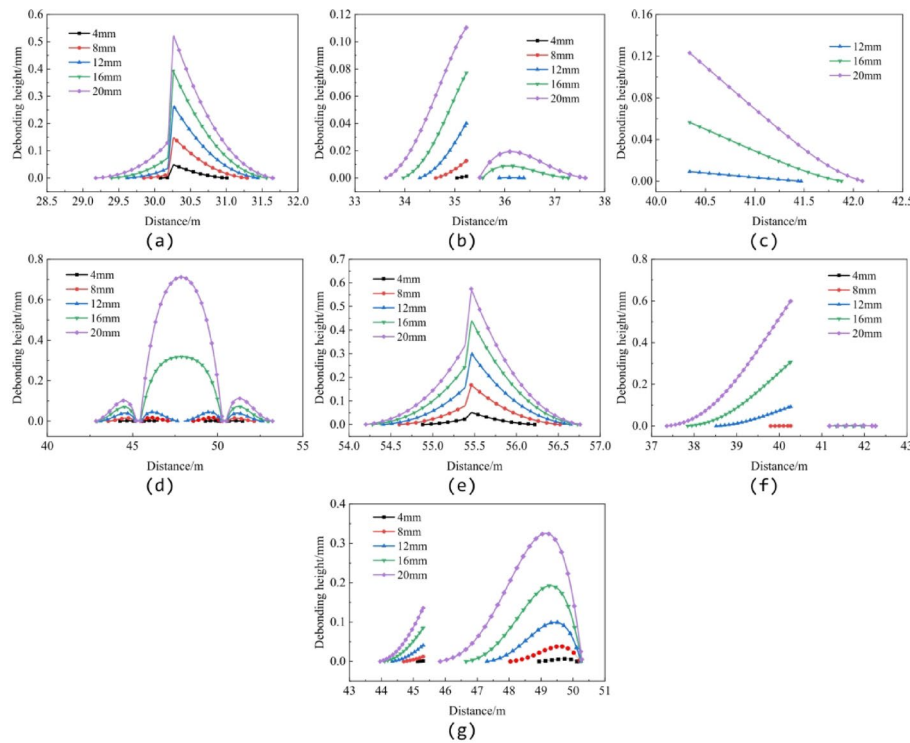


Fig. 10. Longitudinal distribution of the debonding between the track slab-base slab under subgrade settlement. (a) 1#-B3 track slab joint, (b) 1#-B4 track slab joint, (c) 2#-C1 track slab joint, (d) 2#-C2 and C3 track slab joint, (e) 2#-C4 track slab joint, (f) 3#-C1 track slab joint, (g) 3#-C2 and C3 track slab joint.

amplitude is smaller than that away from the position of the settlement amplitude. When the subgrade settlement is at 2[#] position, the interlayer debonding at the C2 and C3 track slab joints shows a left-right symmetrical trend with the position of the settlement amplitude as the symmetry axis. When the settlement amplitude is 4–12 mm, the track slab and the base slab remain in contact at the settlement amplitude. When the settlement amplitude exceeds 12 mm, the two are completely separated in this area, resulting in a rapid increase in both the length and height of the debonding. This occurs because the track slab's deformation reaches the maximum extent that its stiffness can support. After reaching the limit, the impact of the settlement amplitude on the deformation is greatly reduced. However, at this time, the deformation of the base slab is still within the allowable range of stiffness, so the height and length of the debonding between the two layers increase rapidly after the track slab reaches the deformation limit. When the subgrade settlement is at 3[#] position, the larger debonding height is mainly generated at the position of the settlement amplitude and on both sides of the settlement area.

Influence of USS on the contact behavior between the track system and the subgrade system

Figure 11 shows the longitudinal distribution of the debonding between the track system-subgrade system under the subgrade settlement at different positions, indicating that when the subgrade settlement is at 1[#] position, the shape of the two debonding areas is the same. However, the height and length of the debonding are greater near the settlement amplitude position. When the subgrade settlement is at 2[#] position, the debonding between the track system-subgrade system is mainly generated in the slab joint area of the base slab at the position of the settlement amplitude, with the slab joint close to the position of the settlement amplitude being the most affected. When the subgrade settlement is at 3[#] position, the interlayer debonding is symmetrical along the position of the settlement amplitude. With a settlement amplitude of 20 mm, extrusion contact between the track system and the subgrade system persists at the settlement position, so that the debonding height gradually decreases when it is close to the center position. However, As the settlement amplitude further increases, the development of the interlayer debonding in this area is bound to be the same as that shown in Fig. 11 (d), and the height and length of the debonding mutate. On the whole, the interlayer debonding between the track system-subgrade system primarily occurs at the position of the base slab joint and its adjacent track slab joint in the settlement area, but the base slab joint position exhibits the greatest debonding length and height.

Conclusions

Based on the pre-developed general mapping model of the track structure deformation and interlayer contact behavior evolution induced by foundation deformation of HSR, the CSSS description function is implanted, the nonlinear contact between structural layers is considered, and the deformation equation of each layer structure of USBT under CSSS is established. The solutions derived from the theoretical model are compared with the finite

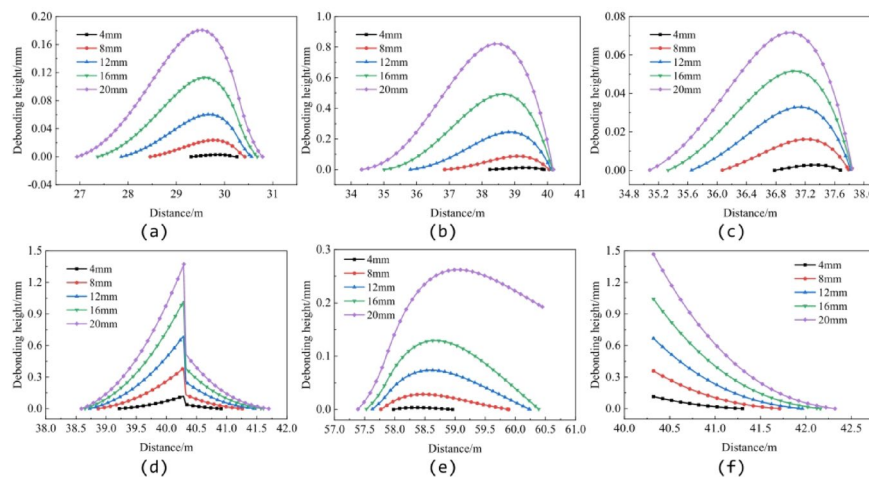


Fig. 11. Longitudinal distribution of the debonding between the track system-subgrade under subgrade settlement. (a) 1#-B3 track slab joint, (b) 1#-Between B3 and B4 track slab joint, (c) 2#-B4 track slab joint, (d) 2#-C1 track slab joint, (e) 2#- Between C4 and D1 track slab joint, (f) 3#-C1 track slab joint.

element model results. The influence of the position of the CSSS on the structure deformation and interlayer contact behavior of each layer of the track is analyzed, and the internal relationship between the interlayer contact force and the contact behavior is revealed. The main conclusions can be summarized as follows:

1. The pre-developed general mapping model, which analyzes track structure deformation and the evolution of interlayer contact behavior caused by foundation deformation of HSR, remains effective for USS analysis when the USS description function is incorporated.
2. When the settlement wavelength of cosine-shaped subgrade is fixed at 20 m and the amplitude increases from 4 mm to 20 mm, the sinking and arching deformation of track structure at each position show a significant linear growth trend. Among them, the increase of the arching deformation of track slab at the slab joint position (1#, 3#) is particularly obvious, and the maximum arching value can reach more than 1.5 times that of the base slab, which is directly related to the reduction of deformation coordination caused by the weakening of structural constraints at the slab joint.
3. The position of the USS deformation significantly affects how track deformation is transmitted within the settlement area. The relative relationship between settlement position and slab joint is the key factor affecting the characteristics of interlayer debonding. When the settlement is located at the slab joint (1#, 3#), the debonding area is symmetrically distributed along both sides of the slab joint, and the debonding height shows the law of “small near settlement end and large far settlement end”. The structural deformation at the position of the slab joint is easily affected by the slab joint, and it is more likely to cause the deformation at the joint position to be inconsistent, resulting in interlayer debonding. Therefore, when studying the influence of foundation damage on USBT, the influence of slab joint should be paid attention to. It is recommended to adopt reinforced joint structure in this area, such as adding shear keys, to improve the anti-deformation ability of the slab joint area.
4. The position of subgrade settlement deformation has a considerably smaller impact on rail deformation compared to its effect on the track slab and base slab. The deformation of both the track slab and base slab is influenced not only by the subgrade settlement position but also closely related to the slab joints. Slab joints are a crucial factor contributing to the uncoordinated deformation of each layer of the track structure.
5. A comparable development pattern is observed for interlayer debonding between the track slab-base slab and the track system-subgrade system. The interlayer debonding between the track-subgrade system primarily occurs at the position of the base slab joint and its adjacent track slab joint in the settlement area, but the length and height of the void at the position of the base slab joint are the largest. That is, as the subgrade settlement amplitude increases, both the height and length of interlayer debonding expand, and the debonding area progressively extends to either side of the slab joint. In addition, the height of the debonding near the position of the settlement amplitude is smaller than that away from the position of the settlement amplitude. It is recommended to lay distributed optical fiber sensors on both sides of the joint, establish a subgrade settlement monitoring system, and identify the risk of debonding in advance in combination with the method in this paper.

However, the parametric study is limited to a specific settlement model, the practical application of this model still needs to be continuously corrected by the long-term measured data of differential settlement of high-speed railway. At the same time, the train load, temperature change and other variables affecting the track structure are not considered, which is also the future optimization direction of the model in this paper. Nevertheless, the model in this paper is still a general tool, which is suitable for track maintenance plan formulation and track component optimization considering subgrade settlement, and can also be used for long-term prediction of the development of track interlayer state.

Data availability

Some or all data, models, or code that support the findings of this study are available from the corresponding author upon reasonable request.

Received: 12 April 2025; Accepted: 18 September 2025
Published online: 14 October 2025

References

- Li, Y. & Conte, J. P. Probabilistic evaluation of seismic isolation effects for a California High-Speed rail prototype Bridge. *J. Struct. Eng.* **145**, 04019136. [https://doi.org/10.1061/\(ASCE\)ST.1943-541X.0002387](https://doi.org/10.1061/(ASCE)ST.1943-541X.0002387) (2019).
- Hubbell, D. & Gauvreau, P. Frequency domain analysis of Train-Guideway interaction dynamics. *J. Struct. Eng.* **144**, 04018100. [https://doi.org/10.1061/\(ASCE\)ST.1943-541X.0002081](https://doi.org/10.1061/(ASCE)ST.1943-541X.0002081) (2018).
- Li, H. L. et al. Fatigue reliability assessment of railway bridges based on probabilistic dynamic analysis of a coupled Train-Bridge system. *J. Struct. Eng.* **142**, 04015158. [https://doi.org/10.1061/\(ASCE\)ST.1943-541X.0001435](https://doi.org/10.1061/(ASCE)ST.1943-541X.0001435) (2016).
- Nie, L. X. et al. A theoretical mapping model for Bridge deformation and rail geometric irregularity considering interlayer nonlinear stiffness. *Steel Compos. Struct.* **46**, 93–105. <https://doi.org/10.12989/scs.2023.46.1.093> (2023).
- Nie, L. X. et al. Mapping relation between rail and Bridge deformation considering nonlinear contact of interlayer. *Materials* **14**, 6653. <https://doi.org/10.3390/ma14216653> (2021).
- Zhou, W. B. et al. Mapping relation between pier settlement and rail deformation of unit slab track system. *Structures* **27**, 1066–1074. <https://doi.org/10.1016/j.istruc.2020.07.023> (2020).
- Chen, Z. W. Relationship between track stiffness and dynamic performance of vehicle-track-bridge system. *Veh. Syst. Dyn.* **59**, 1825–1843. <https://doi.org/10.1080/00423114.2020.1792942> (2021).
- Chen, Z. W., Bi, L. & Zhao, J. W. Comparison of single-pier settlement model and multi-pier settlement model in solving train-track-bridge interaction. *Veh. Syst. Dyn.* **59**, 1484–1508. <https://doi.org/10.1080/00423114.2020.1763406> (2021).
- Chen, Z. W., Zhai, W. M. & Tian, G. Y. Study on the safe value of multi-pier settlement for simply supported girder bridges in high-speed railways. *Struct. Infrastruct. E.* **14**, 400–410. <https://doi.org/10.1080/15732479.2017.1359189> (2018).
- Guo, Y. & Zhai, W. M. Long-term prediction of track geometry degradation in high-speed vehicle-ballastless track system due to differential subgrade settlement. *Soil. Dyn. Earthq. Eng.* **113**, 1–11. <https://doi.org/10.1016/j.soildyn.2018.05.024> (2018).
- Guo, Y., Zhai, W. M. & Sun, Y. A mechanical model of vehicle-slab track coupled system with differential subgrade settlement. *Struct. Eng. Mech.* **66**, 15–25. <https://doi.org/10.12989/sem.2018.66.1.015> (2018).
- Guo, Y., Gao, J. M. & Sun, Y. Mapping relationship between subgrade settlement and rail Deflection of the Double-Block ballastless track. *J. China Railway Soc.* **38**, 92–100. <https://doi.org/10.3969/j.issn.1001-8360.2016.09.014> (2016). (in Chinese).
- Mićić, M. et al. Research on influence of track stiffness on development of rail squat defects. *Proc. Institution Mech. Eng. P I Mech. Eng. F-j Rai.* **239**, 176–186. <https://doi.org/10.1177/09544097241306463> (2025).
- Zhang, X. H., Burrow, M. & Zhou, S. H. An investigation of subgrade differential settlement on the dynamic response of the vehicle-track system. *Proc. Institution Mech. Eng. P I Mech. Eng. F-j Rai.* **230**, 1760–1773. <https://doi.org/10.1177/0954409715613538> (2016).
- Zhong, Y. C., Li, Y. & Zhang, Z. H. Spatial mapping relationship model of subgrade disease and track geometry for high-Speed railway. *Adv. Struct. Eng.* **26**, 888–903. <https://doi.org/10.1177/1369433221145430> (2023).
- Cui, X. & Xiao, H. Interface mechanical properties and damage behavior of CRTS II slab track considering differential subgrade settlement. *Ksce J. Civ. Eng.* **25**, 2036–2045. <https://doi.org/10.1007/s12205-021-0268-6> (2021).
- Cui, X. et al. Effects of lateral differential settlement of the subgrade on deformation behavior and damage evolution of CRTS II slab track. *Eng. Fail. Anal.* **129**, 105674. <https://doi.org/10.1016/j.englfailanal.2021.105674> (2021).
- Xu, Q. Y. & Li, B. Study on Spatial Mechanical Characteristic of High-Speed Railway Ballastless Slab Track on Subgrade. *Adv Mater Res.* **503**–504, 1010–1015. (2012). <https://doi.org/10.4028/www.scientific.net/AMR.503-504.1010>
- Sajjad, M. B. Modelling Transition Zones and Optimal Design Adjoining Tunnels and Bridges. *University of Technology Sydney*, Australia. ISBN: 9798346570943 (2023).
- Wang, H. Y. & Markine, V. Modelling of the long-term behaviour of transition zones: prediction of track settlement. *Eng. Struct.* **156**, 294–304. <https://doi.org/10.1016/j.engstruct.2017.11.038> (2018).
- Shan, Y. et al. Iterative method for predicting uneven settlement caused by High-Speed train loads in Transition-Zone subgrade. *Transp. Res. Record: J. Transp. Res. Board.* **2607**, 7–14. <https://doi.org/10.3141/2607-02> (2017).
- Heydari, H. et al. Investigating the wheel-rail dynamic response of transition system of concrete slab and ballasted tracks through train-track interaction model. *Innov. Infrastruct. So.* **7**, 9. <https://doi.org/10.1007/s41062-024-01538-x> (2024).
- Heydari, H. et al. Performance evaluation of a combined transition system in Slab-Ballasted railway track using a Vehicle-Track-Substructure interaction model. *Ksce J. Civ. Eng.* **9**, 3848–3860. <https://doi.org/10.1007/s12205-023-1273-8> (2023).
- Heydari, H. et al. Field study using additional rails and an approach slab as a transition zone from slab track to the ballasted track. *P I Mech. Eng. F-j Rai.* **4**, 970–978. <https://doi.org/10.1177/0954409717708527> (2018).
- Xiao, W. et al. Effect of uneven subgrade settlement on the CRTS III slab track stress and deformation of high-speed railway. *J. Railway Sci. Eng.* **12**, 724–730 (2015). (in Chinese).
- Feng, Y. L. et al. Rail surface analytical representation of deformation accumulation and stiffness mutation of key components in ballastless track-bridge system induced by earthworks deformation. *China Civil Eng. J.* **56**, 44–57. <https://doi.org/10.15951/j.tmgc.xb.21121200> (2023). (in Chinese).
- Feng, Y. L. et al. Failure mode of interlayer connection of longitudinally-connected ballastless track-bridge system under uneven pier settlement. *Constr. Build. Mater.* **351**, 128805. <https://doi.org/10.1016/j.conbuildmat.2022.128805> (2022).
- Guo, Y., Sun, Q. & Sun, Y. Dynamic evaluation of vehicle-slab track system under differential subgrade settlement in china's high-speed railway. *Soil. Dyn. Earthq. Eng.* **164**, 107628. <https://doi.org/10.1016/j.soildyn.2022.107628> (2023).

Author contributions

Jing Tan: Conceptualization, Investigation, Writing - review & editing. Xuehui Jiang: Validation, Supervision, Re-sources, Funding acquisition. Ruping Luo: Data Curation, Software, Formal analysis. Hongyan Li: Methodology, Software, Roles/Writing-original draft. Shuai He: Data Curation; Software, Formal analysis. Yu Hou: Re-sources, Methodology, Software. All authors listed have contributed sufficiently to the project to be included as authors, and all those who are qualified to be authors are listed in the author byline. All authors reviewed the manuscript.

Declarations

Competing interests

The authors declare that they have no known competing financial interests or personal relationships that could have appeared to influence the work reported in this paper.

Additional information

Correspondence and requests for materials should be addressed to R.L.

Reprints and permissions information is available at www.nature.com/reprints.

Publisher's note Springer Nature remains neutral with regard to jurisdictional claims in published maps and institutional affiliations.

Open Access This article is licensed under a Creative Commons Attribution-NonCommercial-NoDerivatives 4.0 International License, which permits any non-commercial use, sharing, distribution and reproduction in any medium or format, as long as you give appropriate credit to the original author(s) and the source, provide a link to the Creative Commons licence, and indicate if you modified the licensed material. You do not have permission under this licence to share adapted material derived from this article or parts of it. The images or other third party material in this article are included in the article's Creative Commons licence, unless indicated otherwise in a credit line to the material. If material is not included in the article's Creative Commons licence and your intended use is not permitted by statutory regulation or exceeds the permitted use, you will need to obtain permission directly from the copyright holder. To view a copy of this licence, visit <http://creativecommons.org/licenses/by-nc-nd/4.0/>.

© The Author(s) 2025